Quantum well intermixing and MOCVD regrowth for the monolithic integration of 40 Gb/s UTC type photodiodes with QW based components

J. W. Raring, E. J. Skogen, J. S. Barton, C.S. Wang, S. P. DenBaars, and L. A. Coldren

In this letter we present a novel fabrication method for uni-traveling carrier (UTC) type photodiodes using quantum well (QW) intermixing (QWI) and MOCVD regrowth. The fabrication scheme will enable the monolithic integration of the photodiodes with high gain laser diodes, high efficiency electroabsorption modulators (EAM), and high saturation power semiconductor optical amplifiers (SOA). The photodiodes fabricated on intermixed quantum wells presented here exhibit excellent photocurrent handling capabilities, minimal response roll-off over the 20 GHz of our testing capability, and open 40 Gb/s eye diagrams.

Introduction: Monolithic integration of photonic circuits presents tremendous opportunities for the attainment of high-functionality, efficient, compact, and cost effective components for next generation optical networks. Various methods for manipulating the material properties to achieve several QW band edges within a single photonic integrated circuit (PIC) have been reported [1-3]. Beyond this, highly complex PICs will require differing gain or optical confinement at the same or similar wavelength, and in some cases, a radically different internal structure. High-performance multiple QW band-edge widely-tunable PICs have been demonstrated using QWI [4]. With the addition of a single blanket MOCVD step for the growth of an offset multiple QW (o-MQW) active region over an intermixed centered multiple QW (c-MQW) region, we achieved regions of both low and high optical confinement on the same chip [5]. Here we expand on this integration scheme with the demonstration of a uni-traveling carrier (UTC) photodiode fabricated over an intermixed c-MQW active region. This scheme will enable the monolithic integration of the photodiodes with high gain laser diodes, high efficiency EAMs, and high saturation power SOAs. The photodiodes fabricated on intermixed quantum wells exhibit excellent photocurrent handling capabilities, minimal response roll-off over the 20 GHz of our testing capability, and open 40 Gb/s eye diagrams.

With the emergence of fiber amplifiers and the development of SOAs for use in receivers, the demands on photodetectors have drastically increased since they are forced to handle the higher generated photocurrents. The photocurrent handling capabilities of the traditional pin type photodetector is intrinsically limited by the space charge effect, which is a result of the slow carrier transport time associated with the photogenerated holes. The UTC photodiode has been developed specifically to eliminate the influence of hole transport on the performance of the detector. In this type of photodiode, charge transport is governed completely by electrons. The fundamental layers of the UTC are the neutral InGaAs:Zn absorption layer and the depleted wide bandgap InP electron collection layer. Under normal operation, carriers are photogenerated in the absorber layer. The minority carriers (electrons) diffuse towards the collector layer where they accelerate to their overshoot velocity and drift across the collector layer. The escape time of the majority carriers (holes) from the absorption layer is negligible since it is set by the dielectric relaxation time [6]. Thus the carrier transport properties are set solely by electron transport, the space charge effect associated with pin photodiodes is avoided, and saturation current densities 4-6 times higher than that in pin photodiodes are theoretically possible [6].

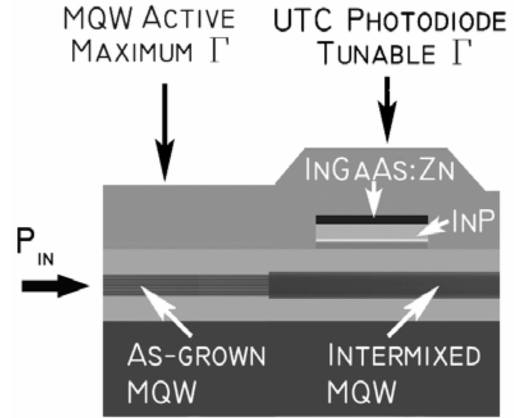

Fig. 1 *Side view schematic of the device structure showing the high confinement c-MQW (left), and the UTC structure grown over regions in which the c-MQW has been intermixed (right).*

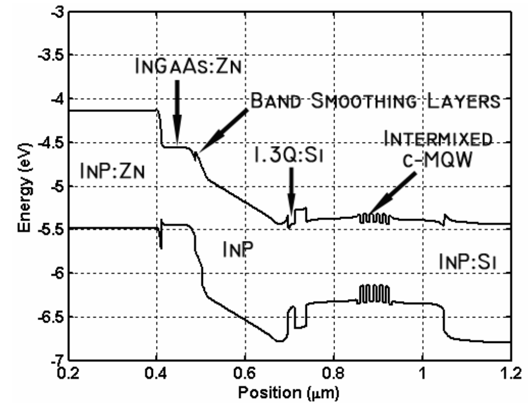

Fig. 2 *Simulated 0 V band diagram for our proposed integrated UTC structure showing the placement of the InGaAs:Zn absorber, conduction band smoothing layers, and InP collector with respect to the intermixed c-MQW.*

Experiment: The epitaxial base structure is grown on a conducting InP substrate using a Thomas Swan Scientific Equipment Ltd. horizontal-flow rotating-disc MOCVD reactor. The active region consists of ten 6.5 nm compressively strained (1.0%) quantum wells, separated by 8.0 nm tensile strained (0.3%) barriers, centered within two InGaAsP:Si (1.3Q:Si) layers designed to maximize the optical confinement in the quantum wells. Following the active region, a 15 nm InP:Si regrowth layer, a 20 nm 1.3Q:Si stop etch, and a 450 nm InP implant buffer layer is grown.

The sample is patterned with Si_xN_y and selectively implanted with P+ for intermixing. Following the implant, the samples are subjected to our QWI process as described in [1]. In the QWI process, the as grown c-MQW is shifted in peak photoluminescence wavelength from 1530 nm to 1410nm in regions where passive waveguide or UTC type detectors are desired. Following the QWI process, the implant buffer layer and 1.3Q stop etch layers are removed using selective wet chemical etching. An MOCVD regrowth is then performed for the growth of a thin InP:Si layer followed by a 1.3Q:Si stop etch layer, a 30nm InP:Si subcollector layer, a 150nm InP collector layer, conduction band smoothing layers, a 50nm InGaAs:Zn absorber layer, and a 200nm InP:Zn cap layer. The epitaxial structure associated with the UTC was based largely on that presented in [6] by Ishibashi et al. The absorber and collector thicknesses were designed to provide 90% quantum efficiency and 3 dB bandwidths in the range of 30 – 40 GHz for a 3 by 25μm diode. Following the regrowth, the sample is patterned with SixNy and a selective wet chemical etch process

is carried out such that the UTC structure remains in regions where it is desired with the blue-shifted c-MQW below. A final MOCVD regrowth is performed to grow the p-type InP:Zn cladding and p-contact InGaAs:Zn layers. A schematic side view illustrating both the high confinement active c-MQW and UTC structure over the intermixed c-MQW regions is presented in Fig. 1. The resulting non-biased band diagram for the UTC region is shown in Fig. 2.

Following the growth of the p-cladding, surface ridge waveguides were defined, photo-benzocyclobutene (BCB) was defined such that it would remain underneath the p-contacts, and p-metal was deposited. The wafers were thinned, back-side n-metalwas deposited, the die were separated into 3 by 25µm diodes, soldered to aluminum nitride carriers, and wire bonded to a matched load of 50 Ω on a coplanar transmission line for RF characterization.

Results: The quantum efficiency of the detectors was estimated by separately reverse biasing two photodetectors configured optically in series. The first detector in the pair is the 25µm detector in question and the second detector is much longer at 250µm such that essentially all optical power escaping the first detector is absorbed. A quantum efficiency of ~90% was estimated by taking the fraction of photocurrent detected in the 25µm detector over the sum of photocurrents in both detectors.

The frequency response of the photodiodes was characterized using a 20 GHz Agilent Lightwave Component Analyzer (LCA). The optical signal from the LCA was fed through an erbium doped fiber amplifier (EDFA) and then coupled into the photodiode waveguide using a tapered fiber. In Fig. 3 the normalized response of the photodiode is shown for various average detected photocurrent levels at a reverse bias of 3 volts. As can be seen in the figure, the 20 GHz response demonstrates under 0.5 dB of roll-off with average photocurrents up to 20 mA. At an average photocurrent of 25mA, the roll off is somewhat increased to 0.75 dB and at 35mA the 20 GHz roll-off is increased to slightly over 2 dB. However, when increasing the reverse bias to 4V (dashed line) at the same average photocurrent, the roll of is decreased to below 1dB.

To examine the large signal characteristics of the photdiodes, eye diagrams were taken at 40 Gb/s in a non-return to zero (NRZ) format using a pseudo-random-bit-sequence (PRBS) of 2^{31}-1. The modulated light was fed through an EDFA and into the waveguide of the photodiode using a tapered fiber. Fig. 4a shows the eye diagrams taken at a 2.5V reverse bias for two different input powers driving a voltage amplitude of 0.33 and 0.41V. As can be seen from the figure, the eye diagrams are open and demonstrate no difference in shape for the two input power levels. In Fig. 4b, eye diagrams are shown for a constant input power at reverse biases of 2.5 and 3.0V. The higher crossing point of the eye diagram driving a voltage amplitude of 0.53V at a reverse bias of 2.5V is indicative of the onset of saturation. However, upon increasing the reverse bias to 3.0V, the voltage amplitude is increased to 0.6V and the crossing point returns to its normal position. The 0.6V amplitude provided by the photodiode at 3V is indicative of a minimum peak current of 24mA in the photodiode.

Conclusion: We have demonstrated UTC type photodiodes using a fabrication scheme ideal for integration with high gain laser diodes, high efficiency EAMs, and high saturation power SOAs using QWI and MOCVD regrowth. The 3 by 25µm photodiodes demonstrated minimal response roll-off over the 20 GHz of our testing capability at a 3V reverse bias and an average photocurrent of 25mA. Open 40 Gb/s eye diagrams were achieved with an amplitude voltage of 0.6V.

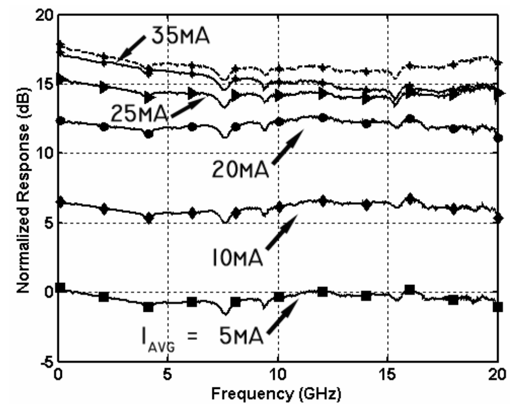

Fig. 3 Optical to electrical response of detector for average photocurrents of 5 (squares), 10 (diamonds), 20 (circles), 25 (triangles), and 35 mA (stars) with a 3V reverse bias (solid lines) and 35mA at a –4V reverse bias (dashed line). Response is normalized to 5mA data set. Markers represent every 80th data point.

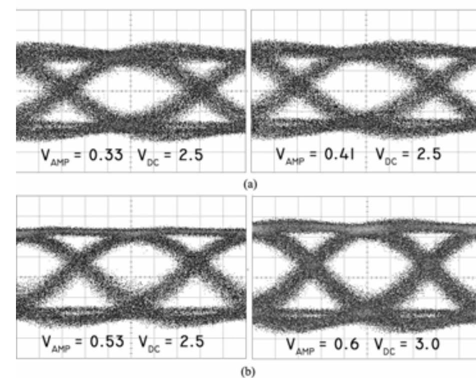

Fig. 4 40 Gb/s eye diagrams from a 25 µm detector at a (a) constant reverse bias of 2.5V and (b) constant input power.

References

[1] E. Skogen, J. Raring, J. Barton, S. DenBaars, and L. Coldren, “Post-Growth Control of the Quantum-Well Band Edge for the Monolithic Integration of Widely-Tunable Lasers and Electroabsorption Modulators,” *IEEE J. Sel. Topics in Quantum Electron*., vol. 9, pp. 1183-1190, September/October, 2003.

2 J. Binsma, P. Thijs, T. VanDongen, E. Jansen, A. Staring, G. VanDenHoven, and L. Tiemeijer, “Characterization of Butt-Joint InGaAsP Waveguides and Their Application to 1310 nm DBR-Type MQW Ganin-Clamped Semiconductor Optical Amplifiers,” *IEICE Trans. Electron*., vol. E80-C, pp. 675-681, 1997.

3 M. Aoki, M. Suzuki, H. Sano, T. Kawano, T. Ido, T. Taniwatari, K. Uomi, and A. Takai, “InGaAs/InGaAsP MQW Electroabsorption Mofulator Integrated with a DFB Laser Fabricated by Band-Gap Energy Control Selective Area MOCVD,” *IEEE J Quantum Electron*., vol. 29, pp. 2088-2096, 1993.

4 J. Raring, E. Skogen, S. DenBaars, and L. Coldren, “Demonstration of negative chirp characteristics over wide wavelength range using monolithically integrated SG-DBR laser electroabsorption modulator,” *IEEE Electronics Letts*. vol.40, pp. 1599-1600 ,2004

5 E. Skogen**,** J. Raring, S. DenBaars, and L. Coldren, “Integration of High-Gain and High-Saturation Power Active Regions using Quantum Well Intermixing and Offset-Quantum Well Regrowth,” *Electron. Lett*., Vol. 40, pp. 993-94, 2004.

6 T. Ishibashi, T. Furuta, H. Fushimi, S. Kodama, H. Ito, T. Nagatsuma, N. Shimizu, and Y. Miyamoto. InP/InGaAs Uni-Traveling-Carrier Photodiodes. *IEICE Trans. Elelctron*., vol. E83-C, no.6 June 2000